



The role of hyperpolarized ^{129}Xe in MR imaging of pulmonary function

Lukas Ebner (M.D.) (Research fellow)^a, Jeff Kammerman (B.S.) (Research Assistant)^b,
Bastiaan Driehuys (Ph.D.) (Professor of Radiology and Biomedical Engineering)^c,
Mark L. Schiebler (M.D.) (Professor of Radiology)^d,
Robert V. Cadman (Ph.D.) (Assistant Scientist)^b,
Sean B. Fain (Ph.D.) (Professor of Medical Physics Radiology and Biomedical Engineering)^{e,*}

^a Cardiothoracic Imaging, Duke University Medical Center, Department of Radiology, Duke University, Durham, NC, USA

^b Department of Medical Physics, University of Wisconsin, Madison, WI, USA

^c Center for In Vivo Microscopy, Duke University, Durham, NC, USA

^d Department of Radiology, University of Wisconsin, Madison, WI, USA

^e Departments of Medical Physics, Radiology, and Biomedical Engineering, University of Wisconsin, Madison, WI, USA

ARTICLE INFO

Article history:

Received 2 September 2016

Accepted 15 September 2016

Keywords:

Polarized gas

Fast MRI

Airway obstruction

Ventilation

Xenon

Oxygen

Fluorinated gases

ABSTRACT

In the last two decades, functional imaging of the lungs using hyperpolarized noble gases has entered the clinical stage. Both helium (^3He) and xenon (^{129}Xe) gas have been thoroughly investigated for their ability to assess both the global and regional patterns of lung ventilation. With advances in polarizer technology and the current transition towards the widely available ^{129}Xe gas, this method is ready for translation to the clinic. Currently, hyperpolarized (HP) noble gas lung MRI is limited to selected academic institutions; yet, the promising results from initial clinical trials have drawn the attention of the pulmonary medicine community. HP ^{129}Xe MRI provides not only 3-dimensional ventilation imaging, but also unique capabilities for probing regional lung physiology. In this review article, we aim to (1) provide a brief overview of current ventilation MR imaging techniques, (2) emphasize the role of HP ^{129}Xe MRI within the array of different imaging strategies, (3) discuss the unique imaging possibilities with HP ^{129}Xe MRI, and (4) propose clinical applications.

© 2016 Elsevier Ireland Ltd. All rights reserved.

long standing solution = forced expiratory volume in one second (FEV₁)

1. Introduction

based on global measurements

For more than a century, the assessment of lung function has relied on global measurements derived from spirometry and body plethysmography [1–3]. Despite its limitations, forced expiratory volume in one second (FEV₁) continues to serve as the main intermediate endpoint in numerous longitudinal studies. As a global measure FEV₁ is not sensitive to disease heterogeneity and is non-specific for the underlying cause of airway obstruction. More generally, traditional pulmonary function tests (PFTs) insufficiently characterize regional lung function in the early stages of disease. Subtle alterations of the lung parenchyma are generally poorly

detected by conventional PFTs; for example, a local loss of ventilation in a given pulmonary segment is missed by these global methods of assessment. Hence, there is a strong demand for more local measures of lung function capable of depicting regional ventilation patterns that are characteristic of different obstructive and restrictive lung diseases in their early stages [4–6].

Imaging technologies have improved the sensitivity and specificity for the detection of lung diseases but without quantification of these processes there has been limited impact outside of the Radiology Department [7]. Chest computed tomography (CT) is considered the reference standard for lung imaging due to its superior spatial and temporal resolution compared to magnetic resonance imaging and nuclear imaging techniques. However, CT excels primarily for lung morphology but relies on indirect signs in cases of obstructive or restrictive pulmonary disease. Interstitial alterations of the lung parenchyma are less conspicuous on CT and are consequently under-diagnosed. However, these very

reference standard for lung imaging = CT

* Corresponding author at: University of Wisconsin – Madison, 2488 Wisconsin Institutes for Medical Research, 1111 Highland Ave., Madison, WI, 53705, USA.

E-mail address: sfain@wisc.edu (S.B. Fain).

subtle, interstitial alterations are critical to the early diagnosis of potentially reversible changes in the lungs [6]. Consequently, there is a pressing need to move beyond form to function in pulmonary imaging.

Thus far, only nuclear imaging methods such as scintigraphy and single positron emission computed tomography (SPECT) are clinically well-established methods to visualize regional ventilation in the setting of the diagnosis of acute and chronic pulmonary embolism [8] and pre-surgical planning of lung volume reduction surgery (LVRS) in COPD [9]. Although several sites have employed SPECT and positron emission tomography (PET) for research applications [10,11], nuclear imaging methods are limited by low resolution, long exam times, and the use of ionizing radiation.

In the attempt to combine the advantages offered by chest CT with ventilation and perfusion assessment, numerous groups have investigated the use of CT with iodinated contrast [12] or with inhaled xenon gas [13] serving as luminal contrast agents. Of note, xenon gas is radiopaque, providing contrast for CT techniques in ventilation and perfusion imaging. Despite the promising results for lung ventilation and brain perfusion yielded by xenon CT, the radiation dose remains an inherent limitation. The risks of medical radiation induced malignancy increase with the accumulated radiation dose [14], imposing practical limits on the role of CT for time-resolved and longitudinal applications unless major dose reductions are realized. As a result, dose reducing CT reconstruction methods are currently an area of intense research [15]. For the foreseeable future patients requiring longitudinal imaging assessment of chronic conditions (i.e. cystic fibrosis, asthma, COPD and lung transplant patients) with a heterogeneous course of disease would benefit the most from radiation free imaging methods.

In light of the aforementioned considerations, MRI has many favorable attributes. Nonetheless, anatomical and physiological properties of the lung parenchyma and the conducting airways represent extreme challenges for MR imaging [16–18]. First, the proton density of normal lung parenchyma is roughly one fifth that of muscle tissue [17]. Second, the air-tissue interface causes a large magnetic susceptibility difference which leads to short T2* relaxation times on the order of 2 milliseconds making diagnostic MR image acquisition of lung parenchyma particularly challenging [17,18]. A third important limitation is sensitivity to motion during the respiratory and cardiac cycles (the heart and the aorta within the field of view) due to the overall longer acquisition time of pulmonary MRI methods [16]. For these reasons lung parenchymal imaging is the “final frontier” of MRI.

An alternative approach is to exploit the many sources of contrast available in MRI to image lung function. Currently available MR scanners paired with state-of-the-art technologies can minimize the impact of the major confounding factors described above. In particular, the introduction of inhaled hyperpolarized (HP) noble gases – specifically xenon-129 (¹²⁹Xe) and helium-3 (³He) – enhances the signal in the lung air spaces sufficiently to enable breath-held images of ventilation with MRI. The hyperpolarization process increases the net nuclear magnetization (and therefore the T₁ signal intensity of the gas) by five orders of magnitude above the thermal equilibrium. Additionally, by inflating the lungs with an MR-visible contrast agent the short T2* of the parenchyma is offset by the increased T2* of the gases inside the alveoli, approximately 20 ms [19], thus improving acquisition efficiency and flexibility for HP gas MRI.

Improvements in MRI acquisition speed stemming from fast parallel imaging and constrained image reconstruction methods has enabled shorter breath-hold times [20,21] and even imaging during dynamic breathing maneuvers [22]. These advances have increasingly improved the feasibility of HP gas MRI methods to explore lung function beyond the morphologic picture derived from CT and the limited global lung assessment of PFTs.

The high cost of HP gas technologies has been a challenge for dissemination of this methodology. One major impediment to the rise of this technology has been the limited availability and high cost of ³He [23]. The isotope is produced as a by-product of the decay of tritium that was used in the production of nuclear warheads in the 1960s and '70s. Moreover, because ³He is an efficient neutron detector, much of its supply has been directed towards this application since 2001 [16,24]. As supply is scarce, ³He faces sharply rising costs. Driven by these drastic economic factors, the transition towards ¹²⁹Xe gas (distilled from the atmosphere) has accelerated.

Concurrent to the ³He-¹²⁹Xe transition, other MRI approaches to lung imaging, such as oxygen enhanced (OE) MRI and perfluorinated (PF) gas MRI have emerged as competitive means to assess for ventilation [25–27]. Each technique has fundamental advantages and inherent limitations [28] with the additional value of OE and PF gases to be determined in larger scale studies. For context, we introduce these techniques, but our primary focus remains on HP ¹²⁹Xe gas MRI. This focus is further motivated by the timely transition of the field from the comparatively rich history of ³He MRI of ventilation to the emerging body of work using ¹²⁹Xe MRI that has been enabled by recent technical advances improving polarization levels and rates [29,30].

There are two purposes to this review. In Section 1, we introduce the most common gas agents that are used for MR imaging of lung ventilation and discuss the advantages and limitations of each method. In Section 2, we review several unique clinical research applications of HP ¹²⁹Xe MRI; we especially emphasize the capability of HP ¹²⁹Xe for spectroscopic imaging of gas exchange.

2. Gas agents for MRI of lung function

The predominant MRI approaches that have been developed to characterize regional ventilation include oxygen-enhanced, PF gases, and the hyperpolarized noble gases ³He and ¹²⁹Xe. This list of HP gases continues to expand as MRI with both hyperpolarized ⁸³Kr [31] and propane-d6 [32] were recently demonstrated. Methodology for imaging of lung function using each gas is treated below with some context to provide a basic understanding of relative strengths and weaknesses of the techniques (Table 1).

2.1. Oxygen-enhanced MRI (OE-MRI) [28]

First reports on oxygen as a contrast agent in pulmonary imaging were published in 1996 [33]. Fundamentally, the inhalation of pure oxygen (100% O₂) simultaneously increases the partial pressure of O₂ in the alveoli, the barrier tissues and the pulmonary capillaries. Due to the paramagnetic properties of oxygen, it decreases T1 relaxation times of protons in the barrier and capillaries. Therefore, using T1 weighted imaging can increase the parenchymal signal to a sufficient degree (on the order of 8–10%) to provide contrast in proportion to the concentration of oxygen in these tissues. Of note, the images resulting from oxygen-enhanced MRI do not directly visualize ventilation itself; images represent oxygen dissolved in both tissues and blood, which reflects the physiology of both ventilation and perfusion [28,34]; For example, the OE effect is seen in the pulmonary venous blood as well as the parenchymal tissues due to oxygen dissolved in the blood returning to the heart (See arrow in Fig. 1).

The advantages of OE MRI are the unlimited supply, the low cost of oxygen gas, and its ready implementation on clinical MR scanners without further modifications. Unlike with hyperpolarized gases, no additional hardware is required.

However, the main disadvantage is substantially longer acquisition times. First, the oxygen effect is not instantaneous. After

Table 1

Overview of gas agents used for MRI of regional lung function [28].

	³ He MRI	¹²⁹ Xe MRI	OE MRI	¹⁹ F MRI
Costs Supply	Very high Low	High good	Low abundant	Average Good
Polarization	30–40%	8–40%	5 ppm ^a	5 ppm ^a
Gas density ^b (g/cm ³)	1.34×10^{-4}	5.75×10^{-3}	1.43×10^{-3}	$6.51\text{--}6.16 \times 10^{-3}$
Volume required (L)	0.25–1.0	0.25–1.0	300	5
Scan length (s)	5–10	5–10	300–1800	12–15
Breath hold	+	+	–	+
Nominal Resolution (mm)	3 × 3 × 10	3 × 3 × 10	2 × 2 × 10	6 × 6 × 15
Ventilation-Weighted	+	+	+	+
Barrier	–	+	(+)	–
RBC	–	+	(+)	–
Gas exchange	–	+	–	–
Microstructure	+	+	–	+
Perfusion	–	+	(+)	–

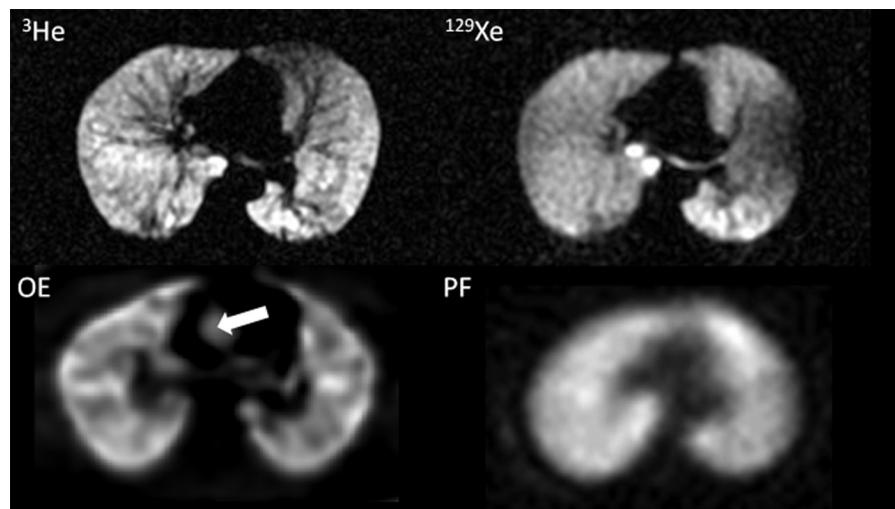
^a Field dependent; values are reported for 1.5 T.^b Gas densities measured at conditions of standard temperature and pressure (STP).

Fig. 1. Example images of the four gas contrast agents: Helium-3, Xenon-129, Oxygen enhanced (OE) and perfluorinated gas (PF). The PF image is adapted from [28]. In the OE contrast image, enhancement extends beyond the lungs into the ascending aorta (arrow). Note that for all the techniques shown a single representative slice is compared from a 3D volume or 2D stack of slices covering the entire lung volume. The OE-MRI example here is using a derivative of ultra-short time to echo (UTE), which significantly improves coverage and resolution for this technique [35].

switching a patient from breathing normoxic gas (21% O₂ and 79% N₂) to 100% O₂, the residual N₂ from the normoxic mixture must wash out of the lung before the full oxygen enhancement can be measured. Estimates of the time to reach the new equilibrium range from 17 to 50 s. Second, signal averaging over multiple breath cycles is required to obtain sufficient SNR. Consequently, this makes the technique prone to respiratory and cardiac motion artifacts. To overcome this, it is necessary to either retrospectively or prospectively respiratory gate the image acquisition. Overall, the combination of the long acquisition times paired with potential motion artifacts and the need for gating make typical OE imaging protocols lengthy. Scan times can be as long as 20 min depending on desired lung coverage and whether dynamic or steady-state oxygen fractions are compared. It should be noted that OE MRI during dynamic wash-in and wash-out has been used to obtain quantitative specific ventilation [36]. Other OE MRI and dynamic imaging approaches using gas agents are discussed in more technical detail in a recent comprehensive review [28]. Most studies use a combination of retrospective and prospective gating and image registration in order to improve the spatial co-registration between the local ventilation and the OE MRI signal.

2.2. Perfluorinated gases [28]

PF = perfluorinated gases

Fluorinated gases, unlike oxygen, are visualized directly as airway contrast agents. As a potential alternative to hyperpolarized ³He and ¹²⁹Xe, PF gas MRI holds promise for assessing regional ventilation. First, due to the high gyromagnetic ratio of fluorine 19 (¹⁹F), the large number of fluorine atoms per molecule of perfluorinated gas, and the short T1 times for PF gases (on the order of a few milliseconds), no external hyperpolarization is needed. Rather, the thermal polarization provided by the magnetic field and rapid signal averaging enable reasonable SNR to be achieved. Second, ¹⁹F has the advantage of being nontoxic and inert; therefore, the application can be considered as safe in human subjects. Furthermore, the natural abundance of fluorine makes it relatively inexpensive compared to hyperpolarized noble gases. Currently, sulfur hexafluoride (SF₆), hexafluoroethane (C₂F₆) and perfluoropropane (C₃F₈) are used as inhaled signal sources for MR ventilation imaging. Of note, scan times with fluorinated gases allow for imaging during a breath-hold, on the order of 12 to 15 s.

However, like for HP gases, dedicated multinuclear transmit and receive radiofrequency coils are required for image acquisition. This substantially raises the initial implementation costs for this

method. Another limitation of this technique is need for somewhat more complex gas delivery. To achieve sufficient SNR, multiple inhalations of the gas mixture, up to several liters inhaled as a normoxic gas mixture, are required in order to reach a detectable gas concentration even for breath-hold imaging. Typically, a single breath hold acquisition (approx. 15 s) is performed but dynamic imaging of gas wash-in and wash-out is also feasible. Nonetheless, these imaging protocols require considerable patient compliance, potentially constraining PF gas techniques in acutely ill subjects unless free-breathing protocols are realized.

2.3. Hyperpolarized gas agents

While the first demonstrations of hyperpolarized MRI used ^{129}Xe gas [37], ^3He was actually the first noble gas to be fully developed, owing to its larger magnetic moment [38], more mature polarization technology, and is chemically and biologically inert. As a consequence, HP ^3He MRI has largely dominated the literature for two decades [39–41].

3. Hardware and gas delivery

Hyperpolarization of noble gases is generally achieved using the spin exchange optical pumping (SEOP) technique [42]. In brief, SEOP is performed in a heated cell of either ^3He or ^{129}Xe gas in mixture with an alkali metal vapor, typically rubidium (Rb), in the presence of a low magnetic field ($\sim 2\text{ mT}$). The cell is irradiated with circularly polarized laser light tuned to a spectral line of Rb to produce spin polarization in the valence electron of the Rb atoms. The Rb electronic polarization is transferred to the noble gas nuclei by collisional spin exchange [24,37]. In practice, polarization fractions of gas nuclei from 20 to 50% can be achieved depending on experimental conditions, vastly improving the achievable signal over conventional thermal polarization from the main magnetic field, i.e. B_0 , of the MRI scanner. These polarizers are now commercially available for research. In addition, the MRI scanner itself must be capable of multi-nuclear scanning. Thus, like the perfluorinated agents, MRI of HP gases requires a broad-band radio frequency (RF) amplifier and receiver hardware typically used for multi-nuclear spectroscopy applications. In addition, HP gas MRI requires transmit/receive coils that are tuned specifically for the gas nucleus of interest; thus, a separate RF-coil would be needed for ^3He versus ^{129}Xe MRI.

Because the signal comes from the gas nucleus itself, MRI with the appropriate hardware can visualize the spin density of the gas distribution during or after inhalation into the lungs without background signal from chest wall or lung parenchymal tissues. Once in contact with oxygen, which is paramagnetic, the T1 relaxation time of the HP gas decreases from $\sim 1\text{--}2\text{ h}$ to $\sim 30\text{ s}$ leading to a need to deliver and image the gas in the lungs within a limited time window. Fortunately, this corresponds well to the typical breath-hold limitations; limiting breath-hold duration is an important safety objective, since ^3He and ^{129}Xe gases are polarized and delivered under anoxic conditions. The HP gases are often diluted in an inert buffer gas such as N_2 . Depending on the study, dilution may have one or more purposes. It allows dose volumes to be standardized to a test subject's lung volume. The dilution fraction for a dose is typically based on the percent polarization of the HP gas to standardize polarization density for each gas dose to mitigate the variation in SNR between subjects. In ^{129}Xe studies, natural helium (^4He) is sometimes used as the buffer, because the combination of the heavy xenon with the light helium produces an average mass closer to that of air, which is more natural for the test subject to inhale. Gases are typically delivered to the test subjects via a gas sampling bag attached to a quick-disconnect one-way valve and filter sys-

tem attached to straw or mouthpiece with a nose clip to avoid nose breathing of air during inhalation (Fig. 2). In some cases, an exhalation tube is included to capture exhaled gases, especially in the case of ^3He gas, which is typically recycled. With state of the art commercial polarizer technology, polarization levels of up to 40% in approximately 20 min are feasible for a typical 1 L dose of HP ^{129}Xe .

4. Overview of imaging applications

Studies using ventilation weighted HP ^3He MRI and ^{129}Xe can depict ventilation impairment in asthma [43–49] and COPD [50–52], with a growing number of recent studies focusing on CF in children [53] and adults [54–56]. As ^3He is confined to the airways and not absorbed by the organism, its application proves safe in patients as well as in healthy volunteers.

The diffusion coefficients of ^3He and ^{129}Xe are also well suited to depict the structures on the scale of the small airways and alveoli (approximately 100–300 μm) using diffusion weighted imaging (DWI) during breath-hold. The technique uses short time constant bi-polar diffusion pulses (e.g. delay times between bi-polar pulses are approximately $\Delta = \delta = 1.5\text{ ms}$) usually placed along the slice encoding direction of a spoiled GRE pulse sequence. The restriction to gas diffusion imposed by the alveolar and small airway structures allows an apparent diffusion coefficient (ADC) to be measured that can quantitatively measure change in small airway and alveolar microstructures due to aging and disease [51,57,58], and emphysema due to tissue loss caused by smoking [59] or α -1-antitrypsin deficiency [51].

5. ^3He vs. ^{129}Xe

In principle, the polarization of ^{129}Xe and ^3He both use SEOP, but with practical differences that affect polarization levels. Unlike for ^3He gas, the xenon interacts much more strongly with the alkali metal vapor used to impart polarization. This strong interaction means that at high pressures (e.g. $>1\text{ atm}$) xenon removes spin from the alkali metal faster than it can be imparted by the laser. This necessitates polarizing xenon in a dilute mixture (1% Xe). Fortunately, this same strong interaction between ^{129}Xe and alkali atoms causes spin exchange polarization to be much more rapid. Therefore, the ^{129}Xe can be polarized during continuous flow through an optical cell and extracted by solidifying the xenon in a cold-finger at liquid nitrogen temperatures. In the frozen state, solid xenon has a theoretical 2–3 h T1 [60], allowing accumulation to practically occur for about 1 h. Once enough HP ^{129}Xe has been accumulated, it is heated to room temperature and sublimated back to the gas phase. This process is maintained under anoxic conditions in a uniform holding field. By optimizing this technique, hyperpolarization levels of ^{129}Xe of up to 40% have been demonstrated, depending on flow rate. Although polarization is still lower than for ^3He , the current state of the art provides sufficient signal to noise ratio (SNR) for robust medical MRI studies.

The SNR of HP ^{129}Xe images of ventilation are slightly inferior to comparable ^3He images (Fig. 1). However, ^{129}Xe gas possesses unique properties that sets it apart from other noble gases. Specifically, xenon is soluble in barrier tissues and blood and exhibits a unique frequency shift that enables it to be distinguished in each of these compartments. These properties were first demonstrated in preclinical rodents and canine models, yielding promising results demonstrating diffusion block to gas exchange in a model of fibrotic lung disease [61] that led to prompt translation into clinical research trials [62,63]. Of note, the physical properties of ^{129}Xe differ substantially from those of ^3He . Specifically, the higher mass of ^{129}Xe affects the flow and physical diffusion characteristics (which

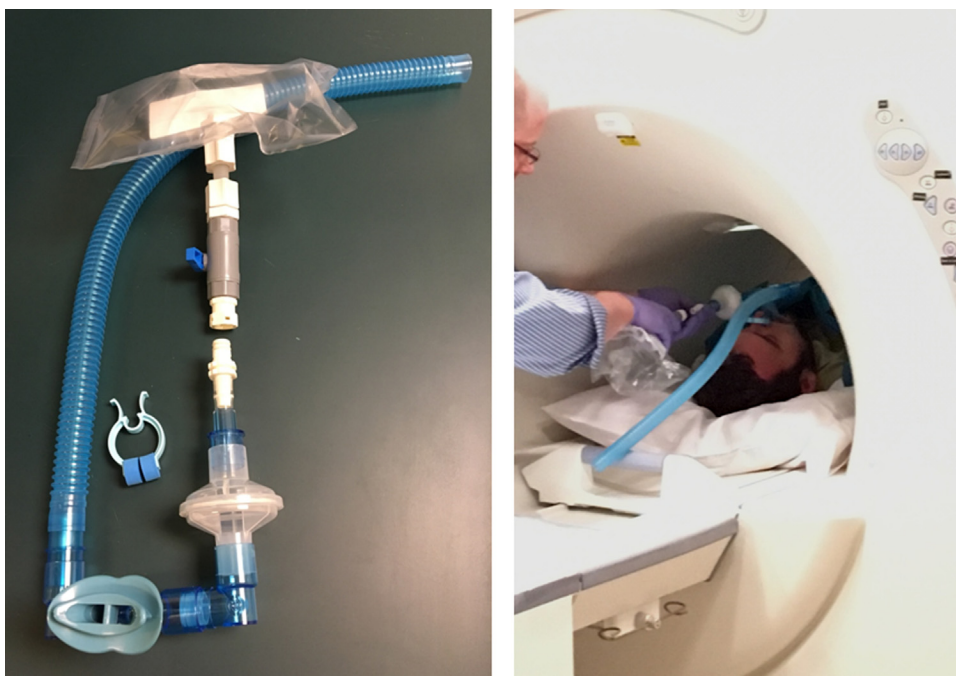


Fig. 2. One system used for delivering hyperpolarized gas to the scan subject. A detailed view is shown on the left, while the right depicts the delivery system in use. The gas bag is attached to the breathing apparatus immediately prior to inhalation and imaging. One-way valves insure that inhaled gas comes from the gas bag, while exhaled gas exits through flexible tubing and is exhausted outside of the scanner bore.

are more comparable to oxygen than are the physical properties of ^3He) resulting in more conspicuous ventilation defects and higher ventilation defect scores than observed with ^3He [64].

Initial testing on patient safety by Driehuys and colleagues proved that administering multiple 1-L doses of pure HP ^{129}Xe to healthy volunteers and patients was well tolerated [62]. In addition there are decades of safe use of ^{133}Xe applied for lung scintigraphy. Since this initial study, numerous other centers have applied this technology safely in different patient populations [56,65,66].

Based on the distribution of ^{129}Xe in the lungs, ventilation impairment could be detected and quantified in several reader-based trials [50,67]. In order to further improve the accuracy of the ventilation quantification, several groups have introduced a semi-automated binning approach [68–70]. By assigning color codes to different signal intensity clusters, an automatized calculation of the ventilation defect percentage (VDP) could be performed (Fig. 3). The semi-automated binning approach has been pursued by several groups in the field [69,70] and appears to be a valuable method when compared to reader assigned ventilation defect scores [68].

Both ^{129}Xe and oxygen gases, but not the highly inert ^3He gas, dissolve along the barrier tissues (i.e. alveolar capillary and alveolar sac) and bind to red blood cells; however, only ^{129}Xe is uniquely identifiable in each of the aforementioned compartments. This is because each compartment presents a different local chemical environment, which causes ^{129}Xe to exhibit a distinct magnetic resonance frequency shifts (Fig. 4). Relative to the gas reference frequency (0 ppm), the barrier tissue resonates at 197 ppm (3.48 kHz at 1.5 T) and the red blood cells (RBCs) at 217 ppm. This phenomenon is exploited with chemical shift imaging techniques that enable local xenon uptake into the lung tissues and red blood cells to be measured as a surrogate for regional gas exchange. In 2010, the first dissolved phase images in humans were acquired with frequency selective RF pulses and a 3-dimensional radial acquisition to overcome the short T_2^* of dissolved ^{129}Xe [71].

6. MRI with HP ^{129}Xe MRI

Typically imaging applications use isotopically enriched ^{129}Xe gas (at least 80% ^{129}Xe , compared to 26% ^{129}Xe in natural Xenon), polarized from 8% to 40% depending on the capabilities of the polarizer on site. Subjects usually inhale between 0.5–1 L of gas from functional residual capacity. Imaging is typically conducted within a single breath hold for both ventilation-weighted and diffusion-weighted applications. After the inhalation of the HP ^{129}Xe , the gas diffuses along the conducting airways and into the respiratory airways as well as the alveoli. Although ^{129}Xe enters the barrier tissues and RBCs almost immediately, the vast majority of the magnetization (~98%) remains in the airspaces. Because the small amount of dissolved magnetization is far off resonance and experiences short T_2^* , a simple fast gradient echo acquisition depicts a pure 3-dimensional ventilation image. As for HP ^3He MRI, HP ^{129}Xe MRI provides 3 dimensional, high resolution ventilation images without the application of ionizing radiation. However, radially acquired imaging can also be valuable for undersampled, isotropic imaging with high SNR [22,73].

For ventilation weighted imaging, defect quantification using VDP – defined as non-ventilated lung volume normalized by the total lung volume – and DWI measuring to quantify alveolar and small airway microstructures are established. As for HP ^3He DWI [74], the semi-quantitative ADC for HP ^{129}Xe MRI is greater in patients with COPD [67] with typical results shown in Fig. 5.

6.1. Ventilation weighted imaging and ventilation defect percentage (VDP)

MRI spin density images of HP ^{129}Xe provide a map of gas distribution in the lungs. These images are able to demonstrate ventilation impairment in a wide array of obstructive pulmonary conditions [50,64,75,76]. The VDP represents the areas of the lung that are not reached by HP gas contrast agents and therefore show

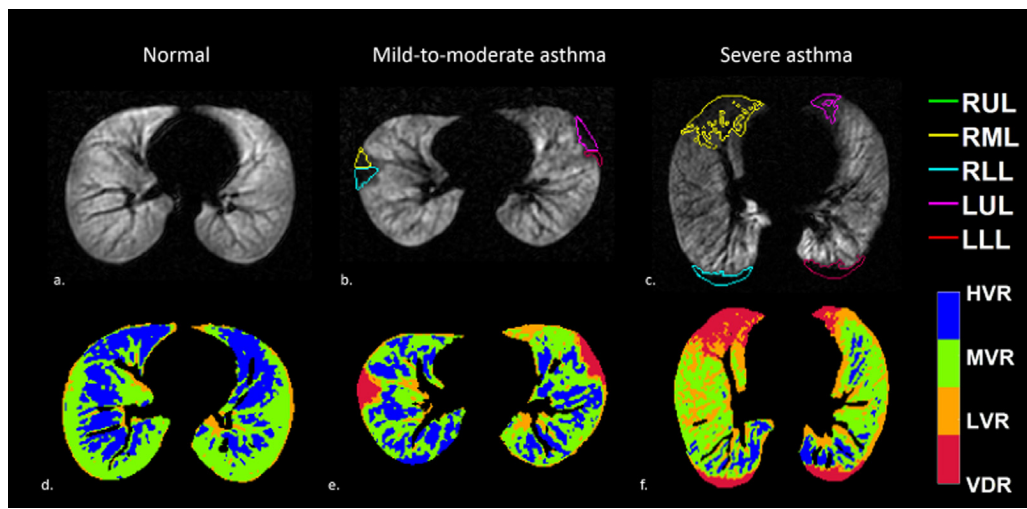


Fig. 3. Typical examples of segmented defects and the corresponding ventilation maps at middle slices of three subjects. The segmented defects for a normal subject (a), mild-to-moderate asthma (b) and severe asthma (c) are outlined with color-coding by lung lobe: right upper lobe (RUL) in green, right middle lobe (RML) in yellow, right lower lobe (RLL) in cyan, left upper lobe (LUL) in magenta, left lower lobe (LLL) in red. In the second row, the corresponding semi-quantitative ventilation maps contain four ventilation levels: the ventilation defect region (VDR) in red, low-ventilated region (LVR) in orange, moderately-ventilated region (MVR) in green, and highly-ventilated region (HVR) in blue.

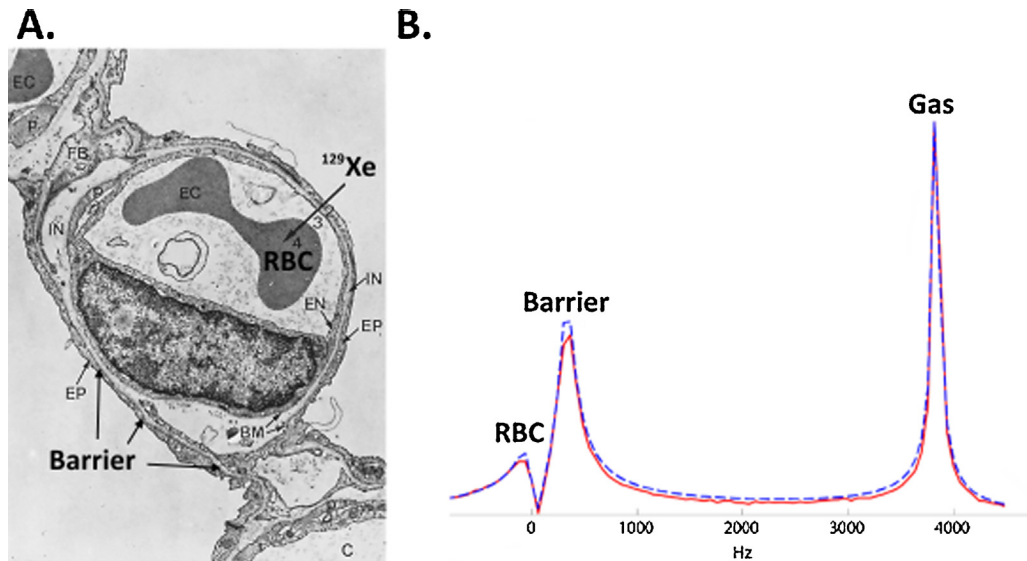


Fig. 4. (A) Electron micrograph of the alveolar-tissue interface (Reproduced with permission from [72]). Septal tissues comprise the liquid lining tissue epithelium (EP), interstitial space (IN), and tissue endothelium (EN). Blood volume comprises the blood plasma, and erythrocyte (EC) – RBC – red blood cell. (B) ^{129}Xe MR spectrum from the human lung with peaks corresponding to the gas, plasma-tissue, and RBC compartments.

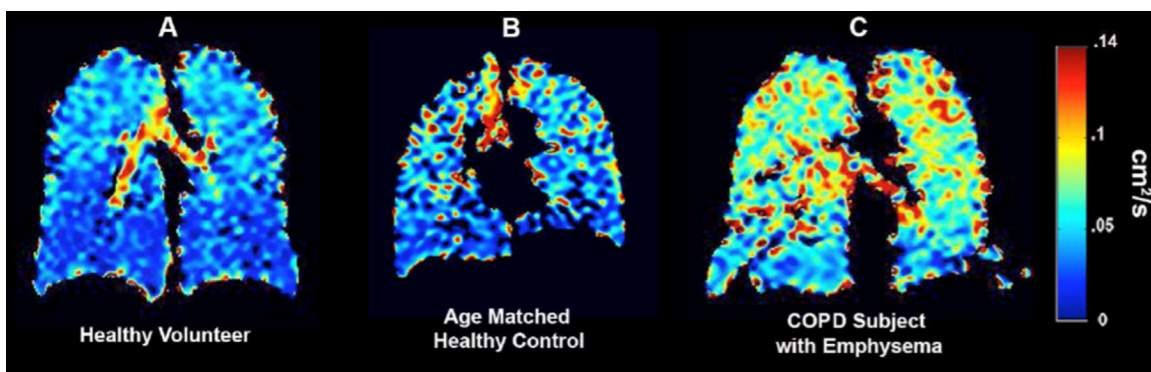


Fig. 5. Apparent diffusion coefficient (ADC) maps for healthy individuals versus COPD. A healthy volunteer (age = 28 years) with a low mean ADC of $0.037 \pm 0.021 \text{ cm}^2/\text{s}$ is depicted in (A); (b) Age matched healthy control; (C) A patient with COPD and previously diagnosed emphysema. ADC values are significantly higher than in the healthy controls ($0.068 \pm 0.028 \text{ cm}^2/\text{s}$); indicating alveolar destruction and a longer path of diffusion in the larger airspaces present in this disease [67].

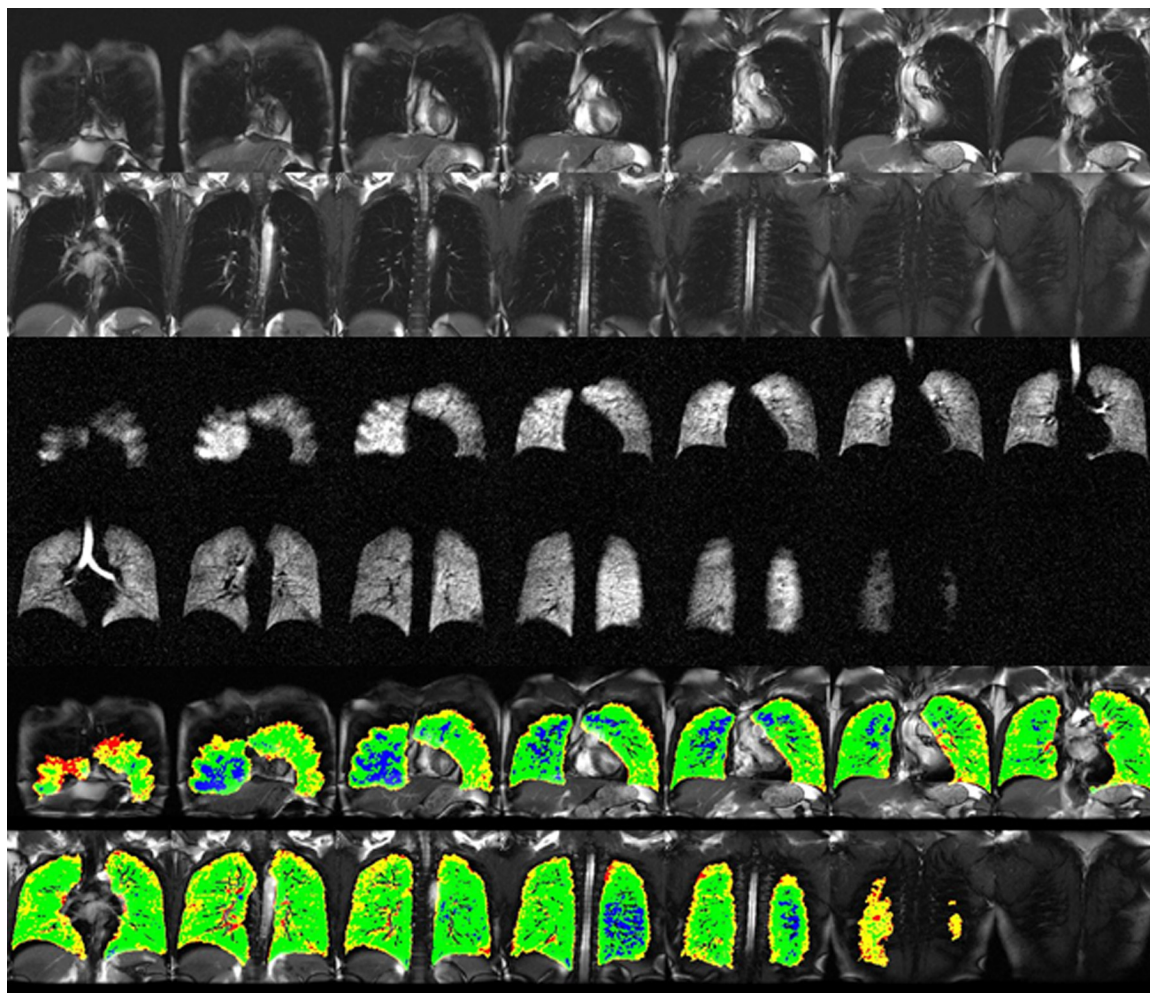


Fig. 6. Healthy, young volunteer imaged anterior to posterior for lung ventilation with MRI. The top two rows show proton MR images that serve as a mask to define the thoracic cavity. The middle two rows show the corresponding normal ^{129}Xe ventilation spin density images. The lowest two rows show linear-binning maps. Ventilation defects are represented by red pixel clusters. Very faint red clusters can be found in the first and last section of the lungs; most likely attributable to partial volume effects during image registration.

Partial volume effects = loss of apparent activity in small objects or regions because of the limited resolution of the imaging system

diminished ventilation and consequently lack of enhancement. Building on techniques developed for quantifying VDP from HP ^3He MRI [70], such measurements are now also readily derived from HP ^{129}Xe MRI. To that end, He and co-workers implemented a semi-automated linear binning approach to further reduce operator dependence, accuracy and increase reproducibility [68]. This linear binning segmentation method has proven useful as a means to objectively quantify the total percentage of non-ventilated lung parenchyma. By rescaling the ^{129}Xe MR images to the 99th percentile of the cumulative distribution and applying fixed thresholds, ^{129}Xe voxels are classified into four clusters: defect, low, medium, and high intensity (Fig. 6). Pixel clusters with low or absent signal intensity represent the VDP.

For HP ^3He MRI, the VDP measure has been investigated in a broad array of obstructive airway diseases including COPD, asthma and cystic fibrosis. In general, the VDP derived from linear binning maps corresponds to reader scores as well as common pulmonary function metrics used for the diagnosis of airway obstruction (FEV₁, functional vital capacity (FVC), FEV₁/FVC) [47,70]. It has been emphasized, that VDP is actually more sensitive to subclinical (regional) airway obstruction showing more dynamic range than global measures of spirometry [77]. Furthermore, VDP shows an age-dependence that is attributable to senile emphysema [78]. However, because PFTs do not provide spatially resolved information, it remains difficult to independently validate HP gas

ventilation MRI. Despite this practical reality HP ^{129}Xe ventilation weighted MRI, the VDP measure, and related regional maps hold potential as biomarkers in future therapy trials based on their empirical associations with outcomes and interventions. Most commonly, ventilation imaging is performed within a single breath-hold. However, dynamic ventilation imaging would enable depiction and measurement of gas flow characteristics like collateral ventilation that may be particularly useful in candidates for luminal lung volume reduction procedures [75].

6.2. Dissolved phase imaging with HP ^{129}Xe MRI

The ability to uniquely identify ^{129}Xe in barrier tissues and RBC by virtue of their strong chemical shifts is arguably the most powerful feature of ^{129}Xe and sets it apart from all other gas imaging agents. These chemical shift frequencies can be detected with spectroscopy and chemical shift imaging (Fig. 7) to quantify the effective gas exchange by taking the relative ratios of the spectral signal peaks within the gas, barrier tissue, and RBC compartments. Such ratios have shown promise as a semi-quantitative measures of global gas exchange impairment and correlate well with clinical tests such as diffusion capacity of carbon monoxide (DLCO) [65,79]. While the total fraction of dissolved ^{129}Xe is only 2% of the total signal at any given instant, Cleveland et al. [80] recognized that the continuous exchange of ^{129}Xe between barrier, RBC,

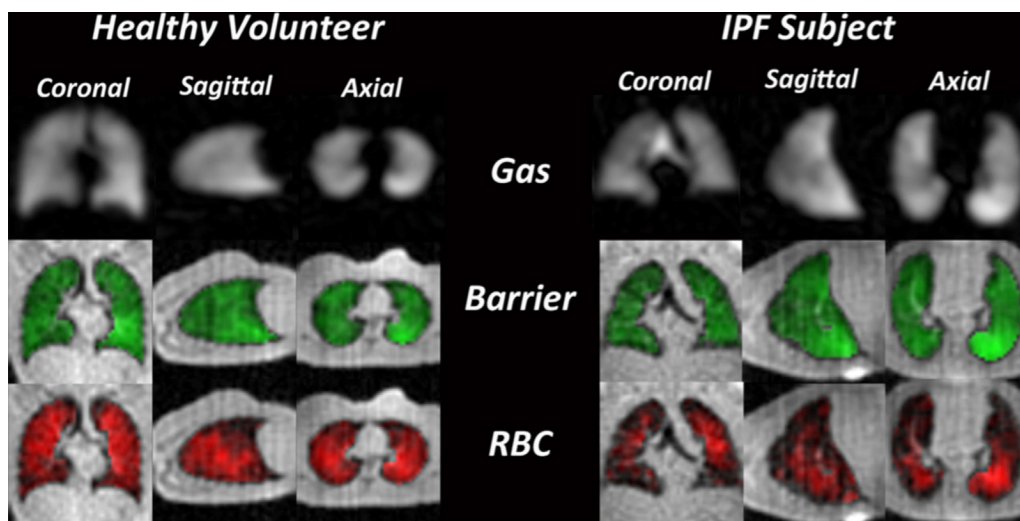


Fig. 7. Representative images of a healthy volunteer and a subject with idiopathic pulmonary fibrosis (IPF). HP ^{129}Xe gas distribution in the lung is depicted in the upper row. No apparent ventilation defects indicating airway obstruction are present. In the middle row, the dissolved Xe gas in the lung interstitium is depicted using a green color. In the healthy volunteer as well as in the IPF patient, the distribution of HP ^{129}Xe in the barrier tissues is homogenous. The HP ^{129}Xe gas bound to red blood cells is pictured in the lower row. Compared to the healthy individual, the IPF subject exhibits substantially decreased HP ^{129}Xe gas in the pulmonary venous blood pool of both lungs. This phenomenon is attributable to interstitial thickening caused by the inflammatory process due to IPF, and as a consequence, gas exchange is reduced [81].

and airspaces permitted this magnetization to be replenished and imaged 3-dimensionally. This has now opened up new avenues for imaging regional gas exchange [81,82].

As pulmonary gas exchange relies on the free diffusion of gases across the alveolar walls, it is evident that any disease that affects these barrier tissues can alter gas exchange. Entities like pulmonary edema, inflammation, scarring, as well as the spread of cancer can impact gas exchange. Any increase in the thickness of these barrier tissues therefore decreases HP ^{129}Xe distribution into them and can impair gas transfer to RBCs.

In 2010, Mugler and colleagues demonstrated imaging of gas uptake in human lungs [83]. This early work was followed by a number of studies exploiting 3-dimensional, radial trajectories with Dixon chemical shift imaging to image the gas-phase and dissolved phase HP ^{129}Xe in one breath hold [81,76]. Pioneering studies by Qing et al. [76] used an innovative multi-spectral radial acquisition based on least-squares reconstruction [84] to demonstrate abnormal barrier tissue to gas and RBC to gas ratios in COPD and asthma. Kaushik and colleagues [81], were likewise able to calculate maps of HP ^{129}Xe transfer from airspaces to the combined barrier and RBC dissolved compartment. This latter study, conducted in healthy individuals only, demonstrated that such maps were sensitive to both lung inflation and posture. Subsequent investigations explored the relation of reduced gas exchange in interstitial pulmonary fibrosis (IPF) and dissolved phase HP ^{129}Xe utilizing gas transfer spectroscopy [79]. The concentration of HP ^{129}Xe in RBCs is markedly reduced in subjects with IPF when compared to healthy subjects (Fig. 7), indicating a net reduction in gas exchange.

These imaging strategies provide regional maps of lung ventilation and gas exchange – the “holy grail” of functional pulmonary imaging – that are strongly correlated with DLCO [76]. The lobar quantification of gas exchange provides a powerful new biomarker for treatment assessment and outcomes in longitudinal studies. This development points towards HP ^{129}Xe functional lung MRI potentially becoming the single most important exam for the evaluation of regional lung function.

Diffusing capacity of the lungs for carbon monoxide (DLCO) is a medical test that determines how much oxygen travels from the alveoli of the lungs to the blood stream

7. Conclusion

HP gas MRI is a robust means to detect and to quantify airway obstruction. For nearly 20 years, hyperpolarized gases have yielded

novel insights into lung physiology and pathology. A trend towards HP ^{129}Xe gas has emerged in the past decade. While initially driven by the shortages of ^3He gas, it is now exposing a potentially far richer set of opportunities that exploit the unique solubility and chemical shift of ^{129}Xe in biological tissues. In the last decade, HP gas MRI has moved from the research labs to the clinics; attracting pulmonologists as well as radiologists in their efforts to more accurately assess regional pulmonary function. By combining ventilation images with gas exchange maps, HP ^{129}Xe MRI is emerging as valuable biomarkers for the longitudinal assessment of medical and surgical therapy for pulmonary disease.

Conflict of interest

The authors declare that Bastiaan Driehuys is founder of Polarean, Inc; and Sean Fain receives grant funding from GE Healthcare.

Acknowledgements

This work was funded in part by NIH/NHLBI R01 HL126771, NIH/NHLBI U10 HL109168, GE Healthcare, financial support to Lukas Ebner by the Swiss National Science Foundation, and NIH/NHLBI R01 HL105643.

References

- [1] J. Hutchinson, On the capacity of the lungs, and on the respiratory functions, with a view of establishing a precise and easy method of detecting disease by the spirometer, *Medico-Chir. Trans.* 29 (1846) 137–252.
- [2] A.B. Dubois, S.Y. Botelho, G.N. Bedell, et al., A rapid plethysmographic method for measuring thoracic gas volume: a comparison with a nitrogen washout method for measuring functional residual capacity in normal subjects, *J. Clin. Invest.* 35 (1956) 322–326, <http://dx.doi.org/10.1172/JCI103281>.
- [3] R. Pellegrino, G. Viegi, V. Brusasco, et al., Interpretative strategies for lung function tests, *Eur. Respir. J.* 26 (2005) 948–968, <http://dx.doi.org/10.1183/09031936.05.00035205>.
- [4] M.R. Sears, Predicting asthma outcomes, *J. Allergy Clin. Immunol.* 136 (2015) 829–836, <http://dx.doi.org/10.1016/j.jaci.2015.04.048>.
- [5] P. Lange, D.M. Halpin, D.E. O'Donnell, W. MacNee, Diagnosis, assessment, and phenotyping of COPD: beyond FEV1, *Int. J. Chron. Obstruct. Pulmon. Dis.* 11 (2016) 3–12, <http://dx.doi.org/10.2147/COPD.S85976>.
- [6] T.J. Doyle, G.M. Hunninghake, I.O. Rosas, Subclinical interstitial lung disease: why you should care, *Am. J. Respir. Crit. Care Med.* 185 (2012) 1147–1153, <http://dx.doi.org/10.1164/rccm.201108-1420pp>.

- [7] K. Sheikh, H.O. Coxson, G. Parraga, This is what COPD looks like, *Respirol Carlton Vic* 21 (2016) 224–236, <http://dx.doi.org/10.1111/resp.12611>.
- [8] K. Kawakami, Topics in pulmonary nuclear medicine, *Ann. Nucl. Med.* 11 (1997) 67–73.
- [9] H. Vesselle, Functional imaging before pulmonary resection, *Semin. Thorac. Cardiovasc. Surg.* 13 (2001) 126–136.
- [10] R.S. Harris, D.P. Schuster, Visualizing lung function with positron emission tomography, *J. Appl. Physiol. (Bethesda, Md. 1985)* 102 (2007) 448–458, <http://dx.doi.org/10.1152/japplphysiol.00763.2006>.
- [11] M.B. Dolovich, D.P. Schuster, Positron emission tomography and computed tomography versus positron emission tomography computed tomography: tools for imaging the lung, *Proc. Am. Thorac. Soc.* 4 (2007) 328–333, <http://dx.doi.org/10.1513/pats.200611-173ht>.
- [12] H.W. Goo, Dual-energy lung perfusion and ventilation CT in children, *Pediatr. Radiol.* 43 (2013) 298–307, <http://dx.doi.org/10.1007/s00247-012-2465-4>.
- [13] W.W. Kim, C.H. Lee, J.M. Goo, et al., Xenon-enhanced dual-energy CT of patients with asthma: dynamic ventilation changes after methacholine and salbutamol inhalation, *AJR Am. J. Roentgenol.* 199 (2012) 975–981, <http://dx.doi.org/10.2214/AJR.11.7624>.
- [14] J.R. Mayo, Radiation dose issues in longitudinal studies involving computed tomography, *Proc. Am. Thorac. Soc.* 5 (2008) 934–939, <http://dx.doi.org/10.1513/pats.200808-079qc>.
- [15] H. Yu, S. Zhao, E.A. Hoffman, G. Wang, Ultra-low dose lung CT perfusion regularized by a previous scan, *Acad. Radiol.* 16 (2009) 363–373, <http://dx.doi.org/10.1016/j.acra.2008.09.003>.
- [16] L.L. Walkup, J.C. Woods, Translational applications of hyperpolarized ^3He and ^{129}Xe , *NMR Biomed.* 27 (2014) 1429–1438, <http://dx.doi.org/10.1002/nbm.3151>.
- [17] H. Hatabu, J. Gaa, E. Tadamura, et al., MR imaging of pulmonary parenchyma with a half-Fourier single-shot turbo spin-echo (HASTE) sequence, *Eur. J. Radiol.* 29 (1999) 152–159.
- [18] H. Hatabu, D.C. Alsop, J. Listerud, et al., T_2^* and proton density measurement of normal human lung parenchyma using submillisecond echo time gradient echo magnetic resonance imaging, *Eur. J. Radiol.* 29 (1999) 245–252.
- [19] X.J. Chen, H.E. Moller, M.S. Chawla, et al., Spatially resolved measurements of hyperpolarized gas properties in the lung in vivo. Part II: T_2^* , *Magn. Reson. Med.* 42 (1999) 729–737, [http://dx.doi.org/10.1002/\(SICI\)1522-2594\(199910\)42:4<729::AID-MRM15>3.0.CO;2-2](http://dx.doi.org/10.1002/(SICI)1522-2594(199910)42:4<729::AID-MRM15>3.0.CO;2-2).
- [20] H.-F. Chan, N.J. Stewart, J. Parra-Robles, et al., Whole lung morphometry with 3D multiple b-value hyperpolarized gas MRI and compressed sensing, *Magn. Reson. Med.* (2016), <http://dx.doi.org/10.1002/mrm.26279>.
- [21] K. Qing, T.A. Altes, N.J. Tustison, et al., Rapid acquisition of helium-3 and proton three-dimensional image sets of the human lung in a single breath-hold using compressed sensing, *Magn. Reson. Med.* 74 (2015) 1110–1115, <http://dx.doi.org/10.1002/mrm.25499>.
- [22] J.H. Holmes, F.R. Korosec, J. Du, et al., Imaging of lung ventilation and respiratory dynamics in a single ventilation cycle using hyperpolarized ^3He MRI, *J. Magn. Reson. Imaging* 26 (2007) 630–636, <http://dx.doi.org/10.1002/jmri.20965>.
- [23] A. Cho, Physics. helium-3 shortage could put freeze on low-temperature research, *Science* 326 (2009) 778–779, <http://dx.doi.org/10.1126/science.326.778>.
- [24] J.E. Roos, H.P. McAdams, S.S. Kaushik, B. Driehuys, Hyperpolarized gas MR imaging: technique and applications, *Magn. Reson. Imaging Clin. N. Am.* 23 (2015) 217–229, <http://dx.doi.org/10.1016/j.mric.2015.01.003>.
- [25] D.O. Kuethe, A. Caprihan, H.M. Gach, et al., Imaging obstructed ventilation with NMR using inert fluorinated gases, *J. Appl. Physiol. (Bethesda, Md. 1985)* 88 (2000) 2279–2286.
- [26] A.F. Halawish, R.E. Moon, W.M. Foster, et al., Perfluoropropane gas as a magnetic resonance lung imaging contrast agent in humans, *Chest* 144 (2013) 1300–1310, <http://dx.doi.org/10.1378/chest.12-2597>.
- [27] Y. Ohno, H. Hatabu, Basics concepts and clinical applications of oxygen-enhanced MR imaging, *Eur. J. Radiol.* 64 (2007) 320–328, <http://dx.doi.org/10.1016/j.ejrad.2007.08.006>.
- [28] S.J. Kruger, S.K. Nagle, M.J. Couch, et al., Functional imaging of the lungs with gas agents, *J. Magn. Reson. Imaging* 43 (2016) 295–315, <http://dx.doi.org/10.1002/jmri.25002>.
- [29] F.W. Hersman, I.C. Ruset, S. Ketel, et al., Large production system for hyperpolarized ^{129}Xe for human lung imaging studies, *Acad. Radiol.* 15 (2008) 683–692, <http://dx.doi.org/10.1016/j.acra.2007.09.020>.
- [30] M.S. Freeman, K. Emami, B. Driehuys, Characterizing and modeling the efficiency limits in large-scale production of hyperpolarized (^{129}Xe), *Phys. Rev. A* 90 (2014) 23406.
- [31] G.E. Pavlovskaya, Z.I. Cleveland, K.F. Stupic, et al., Hyperpolarized krypton-83 as a contrast agent for magnetic resonance imaging, *Proc. Natl. Acad. Sci. U. S. A.* 102 (2005) 18275–18279, <http://dx.doi.org/10.1073/pnas.0509419102>.
- [32] K.V. Kovtunov, M.L. Truong, D.A. Barskiy, et al., Propane-d6 heterogeneously hyperpolarized by parahydrogen, *J. Phys. Chem. C Nanomater Interfaces* 118 (2014) 28234–28243, <http://dx.doi.org/10.1021/jp508719n>.
- [33] R.R. Edelman, H. Hatabu, E. Tadamura, et al., Noninvasive assessment of regional ventilation in the human lung using oxygen-enhanced magnetic resonance imaging, *Nat. Med.* 2 (1996) 1236–1239.
- [34] G. Sommer, G. Bauman, Methoden der MRT zur Ventilations- und Perfusionsbildung der Lunge, *Radiology* 56 (2016) 106–112, <http://dx.doi.org/10.1007/s00117-015-0074-6>.
- [35] S.J. Kruger, S.B. Fain, K.M. Johnson, et al., Oxygen-enhanced 3D radial ultrashort echo time magnetic resonance imaging in the healthy human lung, *NMR Biomed.* 27 (2014) 1535–1541, <http://dx.doi.org/10.1002/nbm.3158>.
- [36] R.C. Sá, M.V. Cronin, A.C. Henderson, et al., Vertical distribution of specific ventilation in normal supine humans measured by oxygen-enhanced proton MRI, *J. Appl. Physiol. (Bethesda, Md. 1985)* 109 (2010) 1950–1959, <http://dx.doi.org/10.1152/japplphysiol.00220.2010>.
- [37] M.S. Albert, G.D. Cates, B. Driehuys, et al., Biological magnetic resonance imaging using laser-polarized ^{129}Xe , *Nature* 370 (1994) 199–201, <http://dx.doi.org/10.1038/370199a0>.
- [38] S. Fain, M.L. Schiebler, D.G. McCormack, G. Parraga, Imaging of lung function using hyperpolarized helium-3 magnetic resonance imaging: review of current and emerging translational methods and applications, *J. Magn. Reson. Imaging* 32 (2010) 1398–1408, <http://dx.doi.org/10.1002/jmri.22375>.
- [39] E.J.R. van Beek, J.M. Wild, H.-U. Kauczor, et al., Functional MRI of the lung using hyperpolarized 3-helium gas, *J. Magn. Reson. Imaging* 20 (2004) 540–554, <http://dx.doi.org/10.1002/jmri.20154>.
- [40] S. Diaz, I. Casselbrant, E. Püttulainen, et al., Validity of apparent diffusion coefficient hyperpolarized ^3He -MRI using MSCT and pulmonary function tests as references, *Eur. J. Radiol.* 71 (2009) 257–263, <http://dx.doi.org/10.1016/j.ejrad.2008.04.013>.
- [41] R.V. Cadman, R.F. Lemanske, M.D. Evans, et al., Pulmonary ^3He magnetic resonance imaging of childhood asthma, *J. Allergy Clin. Immunol.* 131 (2013), <http://dx.doi.org/10.1016/j.jaci.2012.10.032>, 369–376–5.
- [42] T.G. Walker, W. Happen, Spin-exchange optical pumping of noble-gas nuclei, *Rev. Mod. Phys.* 69 (1997) 629–642, <http://dx.doi.org/10.1103/revmodphys.69.629>.
- [43] S.B. Fain, G. Gonzalez-Fernandez, E.T. Peterson, et al., Evaluation of structure-function relationships in asthma using multidetector CT and hyperpolarized ^3He MRI, *Acad. Radiol.* 15 (2008) 753–762, <http://dx.doi.org/10.1016/j.acra.2007.10.019>.
- [44] Y.-S. Tzeng, K. Lutchen, M. Albert, The difference in ventilation heterogeneity between asthmatic and healthy subjects quantified using hyperpolarized ^3He MRI, *J. Appl. Physiol. (Bethesda, Md. 1985)* 106 (2009) 813–822, <http://dx.doi.org/10.1152/japplphysiol.01133.2007>.
- [45] D.J. Niles, S.J. Kruger, B.J. Dardzinski, et al., Exercise-induced bronchoconstriction: reproducibility of hyperpolarized ^3He MR imaging, *Radiology* 266 (2013) 618–625, <http://dx.doi.org/10.1148/radiol.12111973>.
- [46] E.E. de Lange, T.A. Altes, J.T. Patrie, et al., Evaluation of asthma with hyperpolarized helium-3 MRI: correlation with clinical severity and spirometry, *Chest* 130 (2006) 1055–1062, <http://dx.doi.org/10.1378/chest.130.4.1055>.
- [47] S.J. Kruger, D.J. Niles, B. Dardzinski, et al., Hyperpolarized Helium-3 MRI of exercise-induced bronchoconstriction during challenge and therapy, *J. Magn. Reson. Imaging* 39 (2014) 1230–1237, <http://dx.doi.org/10.1002/jmri.24272>.
- [48] T.A. Altes, P.L. Powers, J. Knight-Scott, et al., Hyperpolarized ^3He MR lung ventilation imaging in asthmatics: preliminary findings, *J. Magn. Reson. Imaging* 13 (2001) 378–384.
- [49] S. Samee, T. Altes, P. Powers, et al., Imaging the lungs in asthmatic patients by using hyperpolarized helium-3 magnetic resonance: assessment of response to methacholine and exercise challenge, *J. Allergy Clin. Immunol.* 111 (2003) 1205–1211.
- [50] R.S. Virgincar, Z.I. Cleveland, S.S. Kaushik, et al., Quantitative analysis of hyperpolarized ^{129}Xe ventilation imaging in healthy volunteers and subjects with chronic obstructive pulmonary disease, *NMR Biomed.* 26 (2013) 424–435, <http://dx.doi.org/10.1002/nbm.2880>.
- [51] M. Salerno, E.E. de Lange, T.A. Altes, et al., Emphysema: hyperpolarized helium 3 diffusion MR imaging of the lungs compared with spirometric indexes—initial experience, *Radiology* 222 (2002) 252–260, <http://dx.doi.org/10.1148/radiol.2221001834>.
- [52] M. Kirby, L. Mathew, A. Wheatley, et al., Chronic obstructive pulmonary disease: longitudinal hyperpolarized (^3He) MR imaging, *Radiology* 256 (2010) 280–289, <http://dx.doi.org/10.1148/radiol.10091937>.
- [53] R.P. Thomen, L.L. Walkup, D.J. Roach, et al., Hyperpolarized (^{129}Xe) for investigation of mild cystic fibrosis lung disease in pediatric patients, *J. Cyst. Fibros. Off. J. Eur. Cyst. Fibros. Soc.* (2016), <http://dx.doi.org/10.1016/j.jcf.2016.07.008>.
- [54] M. Kirby, S. Svenningsen, H. Ahmed, et al., Quantitative evaluation of hyperpolarized helium-3 magnetic resonance imaging of lung function variability in cystic fibrosis, *Acad. Radiol.* 18 (2011) 1006–1013, <http://dx.doi.org/10.1016/j.acra.2011.03.005>.
- [55] K. Mentore, D.K. Froh, E.E. de Lange, et al., Hyperpolarized ^3He MRI of the lung in cystic fibrosis: assessment at baseline and after bronchodilator and airway clearance treatment, *Acad. Radiol.* 12 (2005) 1423–1429, <http://dx.doi.org/10.1016/j.acra.2005.07.008>.
- [56] G.A. Paulin, S. Svenningsen, B.N. Jobse, et al., Differences in hyperpolarized (^3He) ventilation imaging after 4 years in adults with cystic fibrosis, *J. Magn. Reson. Imaging* 41 (2015) 1701–1707, <http://dx.doi.org/10.1002/jmri.24744>.
- [57] D.A. Yablonskiy, A.L. Sukstanskii, J.C. Lewoods, et al., Quantitative in vivo assessment of lung microstructure at the alveolar level with hyperpolarized ^3He diffusion MRI, *Proc. Natl. Acad. Sci. U. S. A.* 99 (2002) 3111–3116, <http://dx.doi.org/10.1073/pnas.052594699>.
- [58] S.B. Fain, T.A. Altes, S.R. Panth, et al., Detection of age-dependent changes in healthy adult lungs with diffusion-weighted ^3He MRI, *Acad. Radiol.* 12 (2005) 1385–1393, <http://dx.doi.org/10.1016/j.acra.2005.08.005>.

- [59] S.B. Fain, S.R. Panth, M.D. Evans, et al., Early emphysematos changes in asymptomatic smokers: detection with ³He MR imaging, *Radiology* 239 (2006) 875–883, <http://dx.doi.org/10.1148/radiol.2393050111>.
- [60] B. Saam, Chapter 7: T₁ relaxation of ¹²⁹Xe and how to keep it long, in: *Hyperpolarized Xenon-129*, Magn. Reson. Concepts Prod. Tech. Appl Royal Society of Chemistry, Cambridge, 2015, pp. 122–141.
- [61] B. Driehuys, G.P. Cofer, J. Pollaro, et al., Imaging alveolar-capillary gas transfer using hyperpolarized ¹²⁹Xe MRI, *Proc. Natl. Acad. Sci. U. S. A.* 103 (2006) 18278–18283, <http://dx.doi.org/10.1073/pnas.0608458103>.
- [62] B. Driehuys, S. Martinez-Jimenez, Z.I. Cleveland, et al., Chronic obstructive pulmonary disease: safety and tolerability of hyperpolarized ¹²⁹Xe MR imaging in healthy volunteers and patients, *Radiology* 262 (2012) 279–289, <http://dx.doi.org/10.1148/radiol.11102172>.
- [63] N.J. Stewart, G. Norquay, P.D. Griffiths, J.M. Wild, Feasibility of human lung ventilation imaging using highly polarized naturally abundant xenon and optimized three-dimensional steady-state free precession, *Magn. Reson. Med.* 74 (2015) 346–352, <http://dx.doi.org/10.1002/mrm.25732>.
- [64] S. Svenningsen, M. Kirby, D. Starr, et al., Hyperpolarized ³He and ¹²⁹Xe MRI: differences in asthma before bronchodilation, *J. Magn. Reson. Imaging* 38 (2013) 1521–1530, <http://dx.doi.org/10.1002/jmri.24111>.
- [65] N.J. Stewart, G. Leung, G. Norquay, et al., Experimental validation of the hyperpolarized ¹²⁹Xe chemical shift saturation recovery technique in healthy volunteers and subjects with interstitial lung disease, *Magn. Reson. Med.* 74 (2015) 196–207, <http://dx.doi.org/10.1002/mrm.25400>.
- [66] Y. Shukla, A. Wheatley, M. Kirby, et al., Hyperpolarized ¹²⁹Xe magnetic resonance imaging: tolerability in healthy volunteers and subjects with pulmonary disease, *Acad. Radiol.* 19 (2012) 941–951, <http://dx.doi.org/10.1016/j.acra.2012.03.018>.
- [67] S.S. Kaushik, Z.I. Cleveland, G.P. Cofer, et al., Diffusion-weighted hyperpolarized ¹²⁹Xe MRI in healthy volunteers and subjects with chronic obstructive pulmonary disease, *Magn. Reson. Med.* 65 (2011) 1154–1165, <http://dx.doi.org/10.1002/mrm.22697>.
- [68] M. He, S.S. Kaushik, S.H. Robertson, et al., Extending semiautomatic ventilation defect analysis for hyperpolarized (¹²⁹Xe) ventilation MRI, *Acad. Radiol.* 21 (2014) 1530–1541, <http://dx.doi.org/10.1016/j.acra.2014.07.017>.
- [69] W. Zha, D.J. Niles, S.J. Kruger, et al., Semiautomated ventilation defect quantification in exercise-induced bronchoconstriction using hyperpolarized helium-3 magnetic resonance imaging: a repeatability study, *Acad. Radiol.* 23 (2016) 1104–1114, <http://dx.doi.org/10.1016/j.acra.2016.04.005>.
- [70] M. Kirby, M. Heydarian, S. Svenningsen, et al., Hyperpolarized ³He magnetic resonance functional imaging semiautomated segmentation, *Acad. Radiol.* 19 (2012) 141–152, <http://dx.doi.org/10.1016/j.acra.2011.10.007>.
- [71] S.S. Kaushik, M.S. Freeman, Z.I. Cleveland, et al., Probing the regional distribution of pulmonary gas exchange through single-breath gas- and dissolved-phase ¹²⁹Xe MR imaging, *J. Appl. Physiol.* (Bethesda, Md. 1985) 115 (2013) 850–860, <http://dx.doi.org/10.1152/japplphysiol.00092.2013>.
- [72] Z.I. Cleveland, G.P. Cofer, G. Metz, et al., Hyperpolarized ¹²⁹Xe MR imaging of alveolar gas uptake in humans, *PLoS One* 5 (2010) e12192, <http://dx.doi.org/10.1371/journal.pone.0012192>.
- [73] E.R. Weibel, Morphometric estimation of pulmonary diffusion capacity, *Respir. Physiol.* 11 (1970) 54–75, [http://dx.doi.org/10.1016/0034-5687\(70\)90102-7](http://dx.doi.org/10.1016/0034-5687(70)90102-7).
- [74] M. He, S.H. Robertson, S.S. Kaushik, et al., Dose and pulse sequence considerations for hyperpolarized (¹²⁹Xe) ventilation MRI, *Magn. Reson. Imaging* 33 (2015) 877–885, <http://dx.doi.org/10.1016/j.mri.2015.04.005>.
- [75] M. Salerno, T.A. Altes, J.P. Mugler, et al., Hyperpolarized noble gas MR imaging of the lung: potential clinical applications, *Eur. J. Radiol.* 40 (2001) 33–44.
- [76] H. Marshall, M.H. Deppe, J. Parra-Robles, et al., Direct visualisation of collateral ventilation in COPD with hyperpolarised gas MRI, *Thorax* 67 (2012) 613–617, <http://dx.doi.org/10.1136/thoraxjnl-2011-200864>.
- [77] K. Qing, J.P. Mugler, T.A. Altes, et al., Assessment of lung function in asthma and COPD using hyperpolarized ¹²⁹Xe chemical shift saturation recovery spectroscopy and dissolved-phase MRI, *NMR Biomed.* 27 (2014) 1490–1501, <http://dx.doi.org/10.1002/nbm.3179>.
- [78] D. Pike, M. Kirby, R.L. Eddy, et al., Regional heterogeneity of chronic obstructive pulmonary disease phenotypes: pulmonary (³)He magnetic resonance imaging and computed tomography, *COPD* 13 (2016) 601–609, <http://dx.doi.org/10.3109/15412555.2015.1123682>.
- [79] K. Sheikh, G.A. Paulin, S. Svenningsen, et al., Pulmonary ventilation defects in older never-smokers, *J. Appl. Physiol.* (Bethesda, Md. 1985) 117 (2014) 297–306, <http://dx.doi.org/10.1152/japplphysiol.00046.2014>.
- [80] S.S. Kaushik, M.S. Freeman, S.W. Yoon, et al., Measuring diffusion limitation with a perfusion-limited gas-hyperpolarized ¹²⁹Xe gas-transfer spectroscopy in patients with idiopathic pulmonary fibrosis, *J. Appl. Physiol.* (Bethesda, Md. 1985) 117 (2014) 577–585, <http://dx.doi.org/10.1152/japplphysiol.00326.2014>.
- [81] S.S. Kaushik, S.H. Robertson, M.S. Freeman, et al., Single-breath clinical imaging of hyperpolarized (¹²⁹Xe) in the airspaces, barrier, and red blood cells using an interleaved 3D radial 1-point Dixon acquisition, *Magn. Reson. Med.* 75 (2016) 1434–1443, <http://dx.doi.org/10.1002/mrm.25675>.
- [82] K. Qing, K. Ruppert, Y. Jiang, et al., Regional mapping of gas uptake by blood and tissue in the human lung using hyperpolarized xenon-129 MRI, *J. Magn. Reson. Imaging* 39 (2014) 346–359, <http://dx.doi.org/10.1002/jmri.24181>.
- [83] J.P. Mugler, T.A. Altes, I.C. Ruset, et al., Simultaneous magnetic resonance imaging of ventilation distribution and gas uptake in the human lung using hyperpolarized xenon-129, *Proc. Natl. Acad. Sci. U. S. A.* 107 (2010) 21707–21712, <http://dx.doi.org/10.1073/pnas.1011912107>.
- [84] S.B. Reeder, A.R. Pineda, Z. Wen, et al., Iterative decomposition of water and fat with echo asymmetry and least-squares estimation (IDEAL): application with fast spin-echo imaging, *Magn. Reson. Med.* 54 (2005) 636–644, <http://dx.doi.org/10.1002/mrm.20624>.